Theoretical Review of the Pulse Generation in Dual-Locked Semiconductor Lasers: Asymptotic and Numerical Computation

Erfan Abbaszadeh Jabal Kandi, Khosro Mabhouti, Rahim Naderali*, and Neda Samadzadeh

Department of Physics, Faculty of Science, Urmia University, Urmia, Iran
***Corresponding author email:** r.naderali@urmia.ac.ir

Received: Sept., 12, 2023, Revised: Mar. 1, 2024, Accepted: Apr., 15, 2024, Available Online: Apr. 17, 2024.
DOI: will be added soon

ABSTRACT— In this article, the conditions of pulse production in two mutually coupled lasers are studied. Based on the obtained characteristic equation and its roots, the dynamical behavior of the system and the threshold of the instability are analyzed. For the stable operation of the system and with the use of the time series curves, it is possible to study the dynamical behavior and the stability ranges of the laser in the presence of the saturable absorber and the gain environment. This paper aims to achieve from quasi-periodic behavior in a solitary laser to the generation of a pulse train from two mutually coupled lasers in the presence of saturable absorbers. Also, the stability range for a solitary laser and then for two coupled lasers in the presence of saturable absorbers have been studied.

KEYWORDS: Hybrid mode locking, Numerical analysis, Pulse generation, Stability analysis, Semiconductor laser, Saturable absorber.

I. INTRODUCTION

Continuous stable pulses generation with a long-time interval between pulses is the great possibility for the process of modulation, sending and receiving information [1]. Optical injection and mode locking are the methods to increase the frequency width and dynamics variation [2, 3]. Mode locking in semiconductor lasers can be achieved by active and passive methods [4]. The use of saturable absorbers is included in the passive mode locking methods [5]. The study of saturable absorbers and their applications have been investigated in most common experimental and theoretical studies [6-8]. The primary mechanism of mode locking is easily understood by considering a fast saturable absorber whose absorption can change the pulse width in time scale and shorter pulses. Pulse shortening minimizes laser cavity losses by producing intense pulses [9]. Achieving to the optimal performance for providing industry needs, such as optical telecommunications in the presence of saturable absorbers is the main purpose of this study [10]. Therefore, optimizing laser design in the presence of optical components can be led to stable output of pulse train in a semiconductor laser [11]. With an approach that is based on the optimization of the cavity geometry and cavity design, the amplified amplitude with shorter and more stable pulses can be seen [12, 13, 14].

In this article, at first part, the temporal behavior of the saturable absorber is investigated independently. After that, by introducing the laser output field intensity to the initial combination, the effect of the presence of the saturable absorber exposed to the beam of a single laser is investigated. Finally, in the third part, the operation of the two mutually coupled lasers will be studied in the presence of two saturable absorbers. In all these sections, analytical and numerical solution of the dynamical behavior of the systems, including the stability threshold limit and the characteristic equation have been investigated.

II. SOLITARY LASER

A. *Laser rate equations*

First, the time operation of the saturable absorber has been investigated independently, then by entering the output field intensity of the

laser into the initial combination, the effect of the presence of the saturable absorber exposed to the beam of a single laser (according to Fig. 1) will be investigated. In fact, by studying the characteristics and stable values of a single laser, stability analysis is done for this laser in the presence of an external cavity and a saturable absorber, so that these obtained data are the basis for system studies in the case of two lasers coupled simultaneously. In all these stages, from the two perspectives of analytical and numerical solution, the dynamic behavior of the system, the stability threshold limit and the characteristic equation are the components that will be investigated. To avoid errors in numerical calculations and to eliminate the dependence of calculations on dimensions, we deal with rate equations in dimensionless mode. These equations are dimensionless to the photon lifetime ($\tau_p = 10^{-9}$) and this dimensionless method is taken from the article which was given in [15, 16]. In Fig. 1, a simple schematic of a semiconductor laser in the presence of a saturable absorber is introduced.

To describe the output dynamics of the laser, we use rate equations, which are called Yamada equations [17]. We study a model predicting self-pulsations put forward by Yamada and for experiments with this type of laser, see [18-20]. These Yamada equations represent the temporal changes of field intensity, gain and absorption parameters, which are introduced as follows [21]:

$$\dot{F}_i = \frac{1}{2}(G_i - Q_i - 1)F_i + \sigma_i + \frac{K}{2}(F_{i+1} + F_{i-1} - 2F_i), \quad (1)$$

$$\dot{G}_i = \gamma_i(A_i - G_i - I_i G_i), \quad (2)$$

$$\dot{Q}_i = \gamma_i(B_i - Q_i - a_i Q_i I_i). \quad (3)$$

where F, G, and Q, are respectively, field amplitudes, gain, and absorption, A, B, and a, are respectively, bias current of the gain, background absorption, differential absorption relative to the differential gain, γ, K, and σ are respectively, decay rate of absorption and gain, the exchange of radiation between first-neighbor lasers scaled to the field intensity damping rate of the single laser, and Gaussian noise factor, and $I = |F|^2$ is the field intensity.

The allowed range of parameters used in laser rate equations is presented in Table (1) [18]. In this Section, to check the laser rate equations, (K=0) and (i=1) are taken as default values and the equations are rewritten. It should be noted that in this section the calculations are done without considering the noise (σ=0).

$$\dot{F} = \frac{1}{2}(G - Q - 1)F \quad (4)$$

$$\dot{G} = \gamma(A - G - IG) \quad (5)$$

$$\dot{Q} = \gamma(B - Q - aQI) \quad (6)$$

Table (1) defines the used parameters and their permissible range.

B. *Mathematical model*

Usually, for the analysis of nonlinear systems, it is necessary to obtain a matrix by using the Jacobian matrix [22, 23] and inserting constant values extracted from the equations, which results in the introduction of an equation called the characteristic equation [24] for that system. This equation will be the basis of our following analysis.

1. Calculation of stable values and critical equations

Considering that the main parameters of the laser do not change with time, it is necessary to study the rate of change of its parameters while they are equal to zero to check the dynamics of the laser. These values are called stable values of the system. We set the ($\dot{F}, \dot{G}, \dot{Q}$) values from the rate Eqs. (4, 5, 6) equal to zero and the stable and critical values are obtained.

2. Analytical solution and calculation of characteristic equation

In vector calculus, the Jacobian matrix of a function with several variables is the matrix of all its first-order partial derivatives. When this matrix is square, that is, when the function takes

the same number of variables as input as the number of vector components of its output, its determinant is called the Jacobian determinant. This matrix is often called Jacobin matrix [25]. Using the laser rate equations of all three functions of F, G, and Q variables, their Jacobian matrix, is calculated as follows:

$$J=\begin{pmatrix} \frac{1}{2}(G-Q-1)-\lambda & \frac{F}{2} & -\frac{F}{2} \\ 0 & -\gamma(1+I)-\lambda & 0 \\ 0 & 0 & -\gamma(1+aI)-\lambda \end{pmatrix} \tag{7}$$

Now the determinant of the matrix is calculated to derive the characteristic equation:

$$D=\left(-\gamma\left(1+aI\right)-\lambda\right)\begin{vmatrix} \frac{1}{2}\left(G-Q-1\right)-\lambda & \frac{F}{2} \\ 0 & -\gamma\left(1+I\right)-\lambda \end{vmatrix}=0 \tag{8}$$

By expanding the sentences and sorting them according to powers of λ, the following characteristic equation is obtained:

$$\lambda^3+\lambda^2\left[-\frac{1}{2}(G-Q-1)+\gamma(2+I+aI)\right]+ \\ +\lambda\left[-\frac{\gamma}{2}(G-Q-1)(2+I+aI)+\gamma^2(1+aI)(1+I)\right]+ \\ +\left[-\frac{\gamma^2}{2}(G-Q-1)(1+aI)(1+I)\right]=0 \tag{9}$$

In this way, the resulting roots are λ_1=0.0045, (λ_2=-0.2025 +0.0405i), (λ_3=-0.2025 -0.0405i) the roots of the characteristic Eq. (9) are checked. The desired root should be in the form of (- (R part) + (I part) i). Considering that the roots of the characteristic equation include both real and imaginary parts, the changes in the dynamic behavior of the system can be investigated as shown in Fig. 7 [26]. Therefore, for the characteristic Eq. (9), (λ_2) will be desirable. For the desired roots, the values of the parameters A, B, a, and γ are obtained as (7.4), (5.8), (1.8) and (0.04), respectively, and Fig. 3 is drawn based on them.

C. *System stability analysis*

Finally, to analyze the instability threshold, Hopf bifurcation condition is placed in this equation and separated into two real and imaginary equations [27, 28].

D. *Hopf bifurcation condition*

Now, to check the instability of the system, Hopf bifurcation condition ($\lambda=i\sigma$) is applied (note that (λ) is the eigenvalue of the characteristic Eq. (9)):

$$-i\sigma^3-a\sigma^2+ib\sigma+c=0 \tag{10}$$

The coefficients a, b, and c are known for the characteristic Eq. (9).
Eq. (9) is separated into imaginary and real parts. Its real part is as follows:

$$\sigma^2=\frac{c}{a} \tag{11}$$

Its imaginary part is as follows:

$$-\sigma^3+b\sigma=0 \tag{12}$$

$$\sigma=\pm\sqrt{-\frac{\gamma}{2}\left(G-Q-1\right)\left(2+I+aI\right)+\gamma^2\left(1+aI\right)\left(1+I\right)} \tag{13}$$

To determine the limit of the instability threshold, the root of the characteristic equation ($\lambda=i\sigma$) must be imaginary and always positive so that its maximum value can be obtained and can be chosen as the operating conditions of the system. So, σ must have a real and positive value so that the necessary condition for determining the permissible limit of system instability is established.

E. *Numerical solution*

In this section, we analyze and solve Eqs. (4-6) numerically with the help of Rang-Kuta algorithm [29]. In the absence of laser field

intensity (non-lasing mode), according to the absorption and gain time evolution diagram (Fig. 2), the saturable absorber is repeated. Based on this diagram, the absorption coefficient of the saturable absorber is observed in the range 5.79-5.8 and the average absorption rate is (5.8). The maximum amount of gain is equal to 6.5. As you can see, the time evolution graph is periodic, and this indicates that the system is constantly being absorbed and saturated. Then, by numerically solving the rate equations in the presence of the laser beam, the graph of the time evolution of the output field intensity and the absorption and gain coefficients can be shown in Fig. 3. According to the figure, it can be said that the laser performance is in optimal conditions of periodicity and stability. In fact, for the numerical solution of this structure, we act according to the results obtained from the characteristic Eq. (9). The roots obtained from this characteristic equation provide the desired values for stable operation. So that the range of fluctuations of absorption, gain and laser field intensity is stable. The extraction of the numerical coefficients obtained from the characteristic Eq. (9) will imply that the laser, after starting to work, when it is exposed to the saturable absorber, will behave in such a way that it will have a time evolution in the form of completely dense and periodic pulses. As a result, in this section, the critical equation report and study of dynamics have been done for a single semiconductor laser in the presence of a saturable absorber. In this section, after the time operation of the saturable absorber was studied independently, by introducing the laser output field intensity to the initial combination, the effect of the presence of the saturable absorber exposed to the beam of a single laser was investigated. Also, when the laser is exposed to the saturable absorber after starting to work, the time evolution and dynamics of the system are consistent with the numerical coefficients obtained from the characteristic Eq. (9) (matching in terms of dense and periodic pulses and being in a limit cycle). In general, it was observed that the time width of the laser in the presence of laser field intensity and saturable absorber, compared to the non-lasing mode, decreases and the laser frequency width increases. Also, laser operation is placed in optimal periodic and stable conditions. In the next section, the operation of two coupled lasers in the presence of a saturable absorber and the study of the system dynamics, will be performed with a method similar to this chapter.

F. *Figures, Photographs, and Tables*

In this section, Fig. 1 depicts a simple schematic of a laser cavity in the presence of a gain and saturable absorber. Figure 2 shows the time evolution of absorption (Q) and gain (G) in the non-lasing mode [17], which is modified to continuous wave (CW) mode with quasi-periodic time operation to single-mode periodic operation (see Fig. 3).

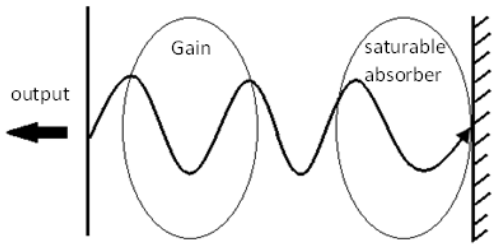

Fig. 1. A simple schematic of a laser in the presence of a gain and saturable absorber.

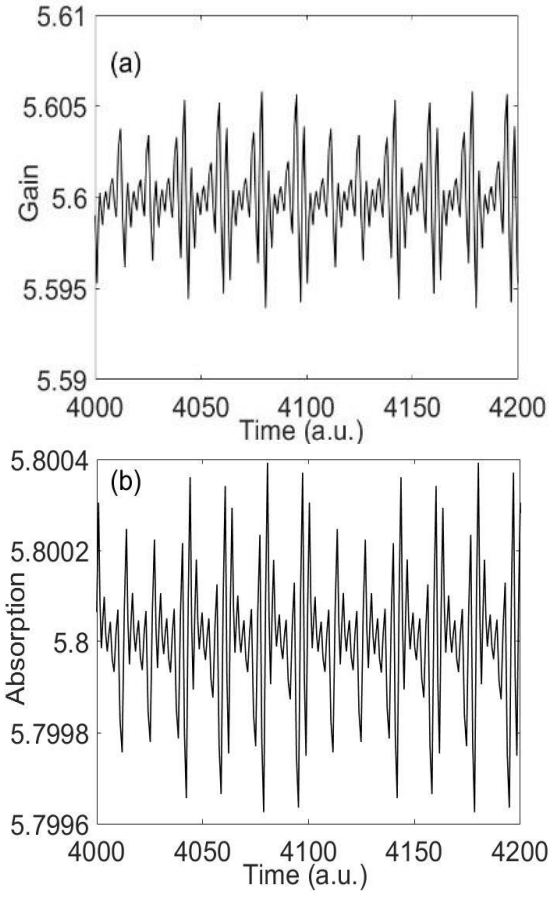

Fig. 2. Time evolution of absorption and gain in the non-lasing mode (absence of laser field intensity (I=0) for numerical values: (γ=0.04, A=5.6, B=5.8, and a=1.8)

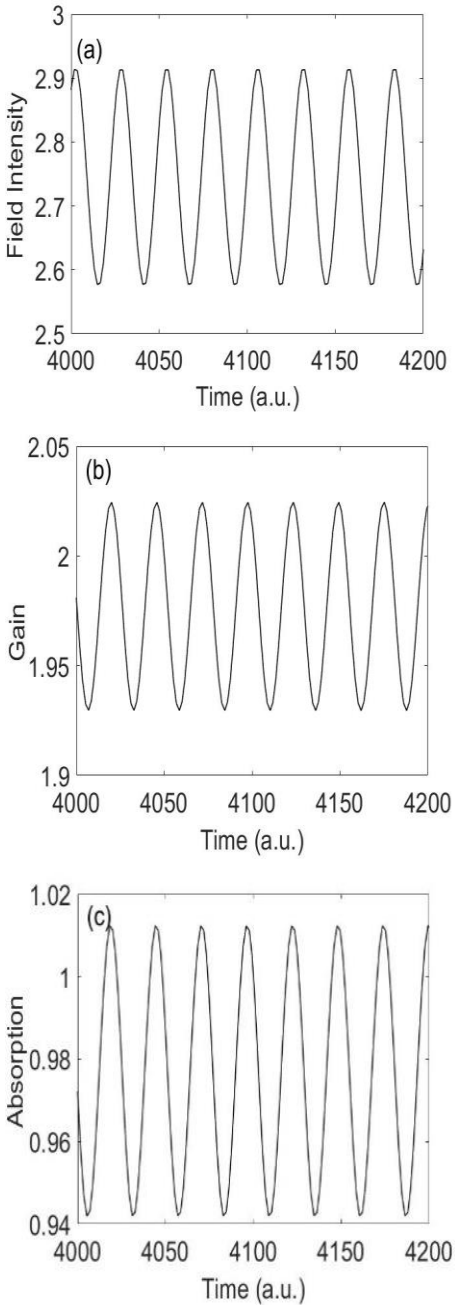

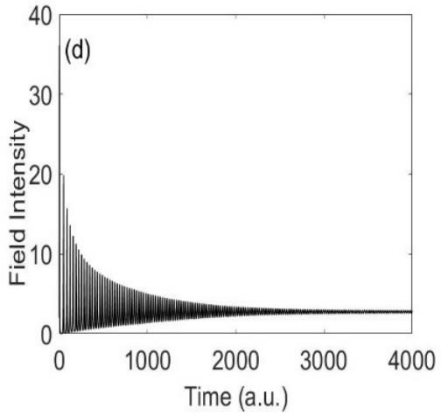

Fig. 3. Time evolution diagram of output field intensity, absorption and gain for a single laser in the presence of laser field intensity for numerical values: (γ=0.04, A=5.6, B=5.8, and a=1.8).

In this cavity (see Figs. 3(a-c)), where the amplifying medium is excited to a sufficiently high level through some optical injection process, the field intensity increases if the unsaturated gain overcomes the losses. After a while, the absorber saturates. The saturation of the absorber leads to an enhanced output power and subsequently to saturation of the gain, which in turn allows the field decay to lower values of field intensity. Then this process repeats itself, which in semiconductor lasers produces a CW [17].

In Fig. 3(d), from a dynamic point of view, the time when the laser starts to evolve based on the given numbers will enter a cycle known as the limit cycle represents the Hopf condition [30].

Table 1. Used parameters and their allowed range.

Parameters	Title	Allowed range
A_i	Bias current of the gain	$Ai \geq 0$
B_i	Background absorption	$Bi \geq 0$
a_i	Differential absorption relative to the differential gain	$ai \geq 1$
γ	Decay rate of absorption and gain	$0 \leq \gamma i < 0.05$

III. TWO MUTUALLY COUPLED LASERS

A. *Laser rate equations*

After the time operation of the saturable absorber was investigated independently in the previous section, by introducing the laser output field intensity to the initial combination,

the effect of the presence of the saturable absorber exposed to the beam of a single laser was investigated. Finally, it was observed that the time evolution of the laser in the presence of laser field intensity and saturable absorber, compared to the absence of the field intensity, decreased and the frequency width of the laser increased. Also, the operation of the laser was placed in the optimal conditions of periodicity and stability. Now, in this section, the operation of the structure based on two mutually coupled lasers (Fig. 4) will be studied in the presence of two saturable absorbers. In all these stages, the components of the dynamic behavior of the system, the threshold limit of stability and the characteristic equation will be investigated from the two perspectives of analytical and numerical solution.

B. *Coupled lasers*

Optical injection locking can improve the laser emission characteristics by enhancing the intrinsic modulation frequency response and by reducing the noise and the frequency chirp [30]. Optically injected coupled lasers induce wide variety of nonlinear dynamical regimes, including pulsation, periodic and chaotic behaviors, and injection locking [31]. As instance, in the secure communication based on coupled laser systems [32], unidirectional coupling or bidirectional coupling, have become a focal point of research for many scholars [33-35]. According to what has been seen in the previous section, one of the most valuable and powerful tools for understanding laser operation is rate equations. In this section, the laser rate equations as are introduced in the previous section (according to relations 1, 2 and 3), this time with the default (i=1), (i=2), and $(K \neq 0)$ are considered and the equations are rewritten. It should also be noted that in this section, calculations are performed without any noise, so (σ=0) [21]:

$$\dot{F}_2 = \frac{1}{2}(G_2 - Q_2 - 1)F_2 + \frac{K}{2}(F_1 - 2F_2) \tag{14}$$

$$\dot{F}_1 = \frac{1}{2}(G_1 - Q_1 - 1)F_1 + \frac{K}{2}(-2F_1 + F_2) \tag{15}$$

$$\dot{G}_2 = \gamma_2\left(A_2 - G_2 - I_2 G_2\right) \tag{16}$$

$$\dot{G}_1 = \gamma_1\left(A_1 - G_1 - I_1 G_1\right) \tag{17}$$

$$\dot{Q}_2 = \gamma_2\left(B_2 - Q_2 - a_2 Q_2 I_2\right) \tag{18}$$

$$\dot{Q}_1 = \gamma_1\left(B_1 - Q_1 - a_1 Q_1 I_1\right) \tag{19}$$

So, with this assumption, there are six rate equations for this coupled laser.

C. *Calculations of stable values and critical relations*

Now, according to the fact that the values of B, a, and γ are constant and according to the rate equations which are considered to be equal to zero, the solutions of the stable state are investigated, and their critical values of absorption and gain are obtained.

D. *Analytical solutions*

The Jacobin matrix is written [28]:

$$J = \begin{pmatrix} \frac{1}{2}(G_1 - Q_1 - 1) - K - \lambda & \frac{K}{2} & \frac{F_1}{2} & 0 & -\frac{F_1}{2} & 0 \\ \frac{K}{2} & \frac{1}{2}(G_2 - Q_2 - 1) - K - \lambda & 0 & \frac{F_2}{2} & 0 & -\frac{F_1}{2} \\ 0 & 0 & -\gamma_1(1 + I_1) - \lambda & 0 & 0 & 0 \\ 0 & 0 & 0 & -\gamma_2(1 + I_2) - \lambda & 0 & 0 \\ 0 & 0 & 0 & 0 & -\gamma_1(1 + a_1 I_1) - \lambda & 0 \\ 0 & 0 & 0 & 0 & 0 & -\gamma_2(1 + a_2 I_2) - \lambda \end{pmatrix} \tag{20}$$

The determinant of the matrix is calculated as:

$$\begin{aligned} D = & \left[\gamma_2\left(1 + a_2 I_2\right) + \lambda\right]\left[-\gamma_1\left(1 + a_1 I_1\right) - \lambda\right] \times \\ & \times \left[\gamma_2\left(1 + I_2\right) + \lambda\right]\left[-\gamma_1\left(1 + I_1\right) - \lambda\right] \times \\ & \times \left[\left(\frac{1}{2}\left(G_1 - Q_1 - 1\right) - K - \lambda\right) \times \right. \\ & \left. \times \left(\frac{1}{2}\left(G_2 - Q_2 - 1\right) - K - \lambda\right) - \frac{K^2}{4}\right] = 0 \end{aligned} \tag{21}$$

Consider that the values of (γ) and (a) are constant:

$$\left[\left(\gamma^2(1+aI_1)(1+I_1)\right)+\left(\gamma\lambda\left(2+I_1(1+a)\right)\right)+\left(\lambda^2\right)\right]\times$$
$$\times\left[\left(\gamma^2(1+aI_2)(1+I_2)\right)+\left(\gamma\lambda\left(2+I_2(1+a)\right)\right)+\left(\lambda^2\right)\right]\times$$
$$\times\left[\left(\frac{1}{4}(G_2-Q_2-1)(G_1-Q_1-1)\right)+\right.$$
$$+\left(-\frac{1}{2}K(G_2-Q_2-1)\right)+\left(-\frac{1}{2}\lambda(G_2-Q_2-1)\right)+$$
$$+\left(-\frac{1}{2}K(G_1-Q_1-1)\right)+(2\lambda K)+$$
$$\left.+\left(-\frac{1}{2}\lambda(G_1-Q_1-1)\right)+\left(\lambda^2\right)+\left(\frac{3}{4}K^2\right)\right]=0 \quad (22)$$

According to the following variables, this determinant is expanded and arranged:

$$(G_1-Q_1-1)=x\ ,\quad \left(2+I_1(1+a)\right)=p\ ,$$
$$(1+aI_1)=m\ ,\quad (1+aI_2)=s,$$
$$(G_2-Q_2-1)=y\ ,\ \left(2+I_2(1+a)\right)=q\ ,$$
$$(1+I_1)=n\ ,\ (1+I_2)=t. \quad (23)$$

Furthermore, based on powers of λ, the characteristic equation of this system is extracted:

$$\lambda^6+\lambda^5\left[\gamma(p+q)+2K-\frac{1}{2}(x+y)\right]+$$
$$+\lambda^4\left[\gamma^2(mn+pq+st)+\gamma\left(-\frac{1}{2}(x+y)+2K\right)\times\right.$$
$$\left.\times(p+q)+\left(\frac{3}{4}K^2-\frac{1}{2}K(x+y)+\frac{1}{4}xy\right)\right]$$
$$+\lambda^3\left[\gamma^3(qmn+pst)+\gamma^2\left(-\frac{1}{2}(x+y)+2K\right)\times\right.$$
$$\left.\times(mn+pq+st)+\gamma\left(\frac{3}{4}K^2-\frac{1}{2}K(x+y)+\frac{1}{4}xy\right)(p+q)\right]+$$
$$+\lambda^2\left[\gamma^4 smtn+\gamma^3\left(-\frac{1}{2}(x+y)+2K\right)(qmn+pst)+\right.$$
$$\left.+\gamma^2\left(\frac{3}{4}K^2-\frac{1}{2}K(x+y)+\frac{1}{4}xy\right)(mn+pq+st)\right]$$
$$+\lambda\left[\gamma^4 smtn\left(-\frac{1}{2}(x+y)+2K\right)+\right.$$
$$\left.+\gamma^3\left(\frac{3}{4}K^2+\frac{1}{4}xy-\frac{1}{2}K(x+y)\right)(qmn+pst)\right]+$$
$$+\left[\gamma^4 smtn\left(\frac{3}{4}K^2-\frac{1}{2}K(x+y)+\frac{1}{4}xy\right)\right]=0 \quad (24)$$

According to Table (1), due to the deficient value of γ [21], we will ignore the decay rate from the second degree onwards for the analysis of this characteristic equation $\left(\gamma^2\approx 0\right)$

However, to analyze the dynamic stability of the system, the characteristic Eq. (24) should be numerically solved. The desired root should be in the form of expression (-(*R* part) + (*I* part) *i*). The roots of the characteristic Eq. (24) are:

$\lambda_1 =$ -0.0549,

$\lambda_2 =$ 0.1449,

$\lambda_3 =$ -1.3576 +*i*0.00002,

$\lambda_4 =$ -1.3576 -*i*0.00002,

$\lambda_5 =$ -0.7719 +*i*0.00002,

$\lambda_6 =$ -0.7719 -*i*0.00002.

Considering that the roots of the characteristic equation including both real and imaginary parts, the changes in the dynamic behavior of

the system can be investigated according to Fig. 7 [26]. As a result, for the characteristic Eq. (24), the roots of λ_3 and λ_5 will be acceptable. For these desirable roots, the values of parameters *A*, *B*, *a*, and γ are obtained as 7.4, 5.8, 1.8 and 0.04, respectively. Figure 5 is plotted based on allowed roots.

E. *System stability analysis*

Similar to the procedure of the previous section for analyzing the instability threshold, Hopf condition is placed in the characteristic Eq. (24) and the equation is divided into real and imaginary equations.

1. Hopf bifurcation condition

First, Hopf bifurcation condition ($\lambda=i\sigma$) is placed, to where λ is an eigenvalue extracted from the characteristic Eq. (24) and σ is a real value:

$$-i\sigma^3 - a\sigma^2 + ib\sigma + c = 0 \tag{25}$$

Eq. (24) is separated in terms of being real or imaginary. The real part is as follows:

$$\sigma^2 a = c \tag{26}$$

The imaginary part is as follows:

$$-\sigma^3 + b\sigma = 0 \tag{27}$$

According to Hopf bifurcation condition ($\lambda=i\sigma$), to determine the instability threshold, the root of the characteristic equation must be imaginary and positive, and the system must be oscillatory unstable. Otherwise, if the root of the equation is negative, it will be a stable fluctuation, which is undesirable. Therefore, the limit of the instability threshold should be specified, and the permissible limit of the system can be determined. Hence, according to the imaginary part, the stability of the system can be investigated:

$$\sigma = \pm\sqrt{b} \tag{28}$$

As we said, to determine the limit of the instability threshold of the root of the characteristic equation ($\lambda=i\sigma$), it must be imaginary and always positive in order to obtain the maximum value that can be chosen as the operating conditions of the system. So, σ must have a real and positive value so that the necessary condition for determining the permissible limit of system instability is established. Thus, only the positive value of σ is acceptable. Therefore, it should always be $(b \geq 0)$:

$$\gamma\left(-\frac{1}{2}(x+y)+2K\right)(p+q)+\left(\frac{3}{4}K^2-\frac{1}{2}K(x+y)+\frac{1}{4}xy\right)\geq 0 \tag{29}$$

F. *Numerical solution*

In this section, the system with two pairs of mutual lasers in the presence of two saturable absorbers are considered. Eqs. (14 to 19) are also analyzed and solved numerically with the help of Rang-Kuta algorithm and MATLAB software [29, 36]. By choosing the appropriate numbers from the characteristic Eq. (24), the combination of two lasers will tend toward the limit cycle. Finally, it will have completely periodic behavior with a constant maximum amplitude level. Due to the presence of two coupled lasers, it is observed that the time intervals are stable, and the continuous pulses are more amplified.

what can be seen in (Fig. 3(a)) is different from two aspects compared to (Fig. 5(c)). First, the laser field intensity is well amplified, and secondly, according to the (Fig. 5(c)) and (Fig. 5(f)) (due to the optical injection) as expected, the time period of the field intensity is shorter and the time interval between the pulses is increased. Considering the time, this issue will be an extra ordinary possibility in the process of modulation and sending and receiving information, the possibility of modulating and loading information on pulses is possible, and this issue is significant from a practical point of view. As a result, after injecting the laser output into the initial combination in the previous section, the effect of the presence of a saturable absorber exposed to the beam of a single laser was studied. In this section, the operation of the structure based on two mutually coupled lasers in the presence of

two saturable absorbers, the dynamic behavior of the system, the stability threshold limit and its characteristic equation were investigated from both analytical and numerical solution perspectives.

G. *Figures, Photographs, and Tables*

In this section, Fig. 4 shown a simple schematic of two mutually coupled lasers in the presence of two saturable absorbers.

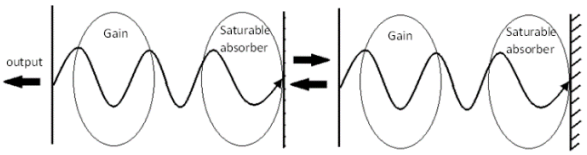

Fig. 4. A simple schematic of two mutually coupled lasers in the presence of two gain and two saturable absorbers.

In Fig. 3 the waves are continuous, but in Fig. 5 due to the presence of two mutually coupled lasers, there are pulse dynamics and amplified continuous pulses. It can also be seen that compared to (Fig. 2), the output of (Fig. 5) is placed in desirable conditions of absorption and gain. The noteworthy point is that in terms of time, far more separable pulses will be obtained in the output.

Figure 6(a) shows the frequency width of spontaneous transitions in non-lasing mode. Figure 6(b) shows the frequency variation of the pulse train. According to Fig. 6(a), in the gain medium, all laser modes (side modes) can grow in the gain medium spontaneously. Meanwhile in pulse train operation only the main mode can be amplified.

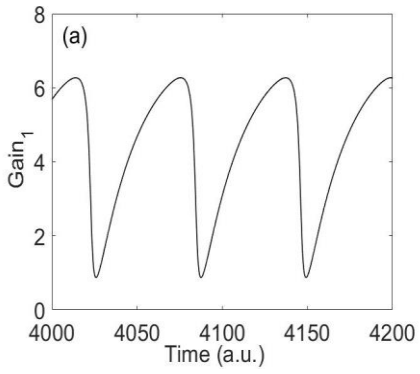

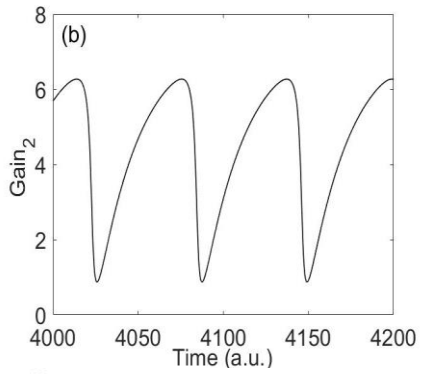

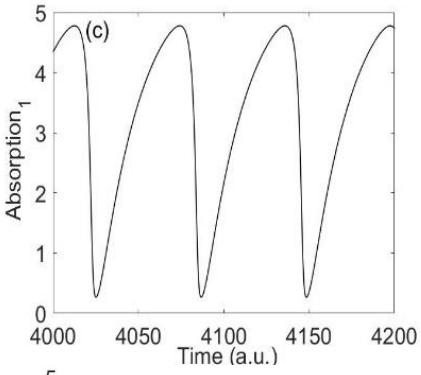

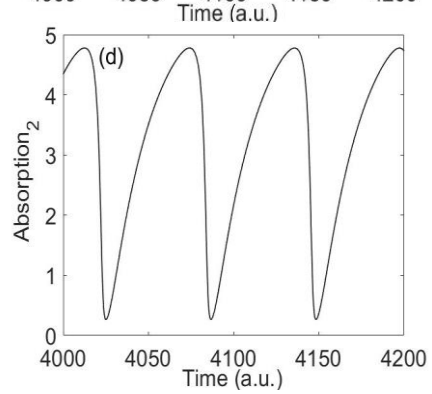

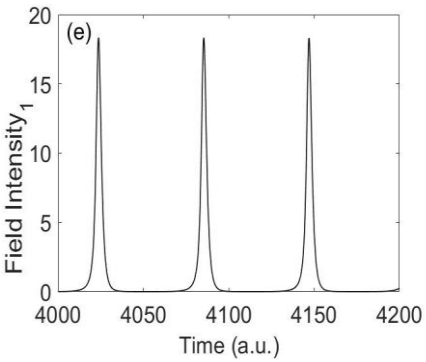

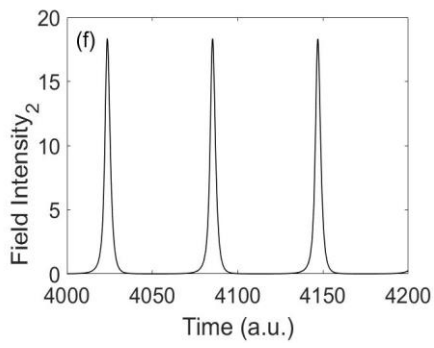

Fig. 5. Time evolution of absorption, Q and gain (G) and laser field intensity (I) in terms of time in two mutually coupled lasers with numerical values: (γ=0.04, A=5.6, B=5.8, a=1.8).

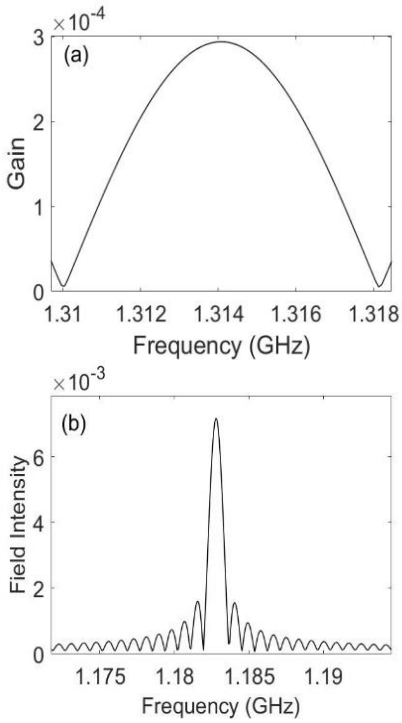

Fig. 6. Fast Fourier Transform of: (a) gain medium (non-lasing mode). (b) laser field intensity (pulse train)

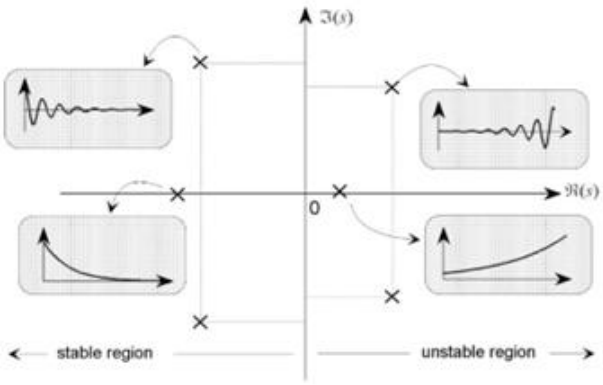

Fig. 7. The type of dynamic behavior of the system according to the positive and negative areas of the real and imaginary parts of the roots [26].

IV. Conclusion

In conclusion, first the saturable absorber's temporal behavior was independently observed. While the system is periodically absorbing and saturating, it does not have any pulse output (non-lasing mode). However, when it is exposed to the laser beam, it can have a continuous and stable output. Optical injection is a factor that increases the frequency width and changes the dynamics. Therefore, it is observed that there are more amplified pulses with a higher frequency width (shorter time width) and a more proportional separability between two output pulses. In other words, based on the critical domains and critical relations obtained from the characteristic equations derived from the laser rate equations, we obtain the allowed and non-virtual regions, which provide stable and unstable operation for a laser-absorber combination. The calculations performed in this article make it possible to have a correct insight into the effect of various parameters on the stable operation of the laser-absorber without laboratory tests.

References

[1] A. Elbaz, D. Buca, N. von den Driesch, K. Pantzas, G. Patriarche, N. Zerounian, E. Herth, X. Checoury, S. Sauvage, I. Sagnes, and A. Foti, "Ultra-low-threshold continuous-wave and pulsed lasing in tensile-strained GeSn alloys." Nature Photon., Vol. 14, pp. 375-382, 2020.

[2] M.M. Sheikhey, R. YadiPour, and H. Baghban, "Promotion of temperature-dependent characteristics of midinfrared quantum cascade lasers under optical injection locking," Phys. Rev. A, Vol. 100, pp. 053856 (1-9), 2019.

[3] Y. Han, Y. Guo, B. Gao, C. Ma, R. Zhang & H. Zhang, "Generation, optimization, and application of ultrashort femtosecond pulse in mode-locked fiber lasers," Prog. in Quantum Electron., Vol. 71, pp. 100264 (1-35), 2020.

[4] J. Lee, H. Chung, J. Koo, G. Woo, and J.H. Lee, "A 3-D printed saturable absorber for femtosecond mode-locking of a fiber laser," Opt. Mater., Vol. 89, pp. 382-389, 2019.

[5] C. Rulliere, *Femtosecond laser pulses*, Springer, pp. 28-32, 2005.

[6] S.Y. Set, H. Yaguchi, Y. Tanaka, and M. Jablonski, "Laser mode locking using a saturable absorber incorporating carbon nanotubes," J. lightw. Technol., Vol. 22, pp. 51-56, 2004.

[7] M.A. Larotonda, A. Hnilo, J.M. Mendez, and A.M. Yacomotti, "Experimental investigation on excitability in a laser with a saturable absorber," Phys. Rev. A, Vol. 65, pp. 033812 (1-6), 2002.

[8] K.Y. Lau, X. Liu, and J. Qiu, "MXene saturable absorbers in mode-locked fiber laser," Laser Photon. Rev., Vol. 16, pp. 2100709, 2022.

[9] J. He, H. Lu, L. Tao, y. Zhao, Z. Zheng, and B. Zhou, "Nonlinear optical properties of PtTe 2 based saturable absorbers for ultrafast photonics," J. Mater. Chem. C, Vol. 10, pp. 5124-5133, 2022.

[10] A.R. Muhammad, R. Zakaria, M.T. Ahmad, P. Wang, and S.W. Harun, "Pure gold saturable absorber for generating Q-switching pulses at 2 μm in thulium-doped fiber laser cavity," Opt. Fib. Technol., Vol. 50, pp. 23-30, 2019.

[11] T. Wang, X. Jin, J. Yang, J. Wu, Q. Yu, Z. Pan, H. Wu, J. Li, R. Su, J. Xu, and K. Zhang, "Ultra-stable pulse generation in ytterbium-doped fiber laser based on black phosphorus," Nanoscale Adv., Vol. 1, pp. 195-202, 2019.

[12] B. Liu, H. Bromberger, A. Cartella, T. Gebert, M. Först, and A. Cavalleri, "Generation of narrowband, high-intensity, carrier-envelope phase-stable pulses tunable between 4 and 18 THz," Opt. Lett., Vol. 42, pp. 129-131, 2017.

[13] G.P. Agrawal, *Nonlinear fiber optics. In Nonlinear Science at the Dawn of the 21st Century*, Springer, pp. 195-211, 2000.

[14] K.Y. Lau, P.J. Ker, A.F. Abas, M.T. Alresheedi, and M.A. Mahdi, "Long-term stability and sustainability evaluation for mode-locked fiber laser with graphene/PMMA saturable absorbers," Opt. Commun., Vol. 435, pp. 251-254, 2019.

[15] R. Lang and K. Kobayashi, "External optical feedback effects on semiconductor injection laser properties," IEEE J. Quantum Electron., Vol. 16, pp. 347-355, 1980.

[16] P.M. Alsing, V. Kovanis, A. Gavrielides, and T. Erneux, "Lang and Kobayashi phase equation," Phys. Rev., A, Vol. 53, pp. 4429(1-6), 1996.

[17] J.L.A. Dubbeldam and B. Krauskopf, "Self-pulsations of lasers with saturable absorber: dynamics and bifurcations," Opt. Commun., Vol. 159, pp. 325-338, 1999.

[18] S. Terrien, B. Krauskopf, and N.G.R. Broderick, "Bifurcation analysis of the Yamada model for a pulsing semiconductor laser with saturable absorber and delayed optical feedback," SIAM J. Appl. Dynamic. Systems, Vol. 16, pp. 771-801, 2017.

[19] V.A. Pammi, K. Alfaro-Bittner, M.G. Clerc, and S. Barbay, "Photonic computing with single and coupled spiking micropillar lasers," IEEE J. Select. Top. Quantum Electron., Vol. 26, pp. 1500307(1-7), 2019.

[20] F. Selmi, R. Braive, G. Beaudoin, I. Sagnes, R. Kuszelewicz, T. Erneux, and S. Barbay, "Spike latency and response properties of an excitable micropillar laser," Phys. Rev. E, Vol. 94, pp. 042219(1-8), 2016.

[21] A.M. Perego and M. Lamperti, "Collective excitability, synchronization, and array-enhanced coherence resonance in a population of lasers with a saturable absorber," Phys. Rev. A, Vol. 94, pp. 033839(1-5), 2016.

[22] M.R. Eslahchi, M. Dehghan, and S. Ahmadi_Asl, "The general Jacobi matrix method for solving some nonlinear ordinary differential equations," Appl. Math. Modelling, Vol. 36, pp. 3387-3398, 2012.

[23] X. Wang, W. Zhu, and X. Zhao, "An incremental harmonic balance method with a general formula of Jacobian matrix and a direct construction method in stability analysis of periodic responses of general nonlinear delay differential equations," J. Appl. Mech., Vol. 86, pp. 061011(1-11), 2019.

[24] N.A. Andriyanov and Y.N. Gavrilina, "Image models and segmentation algorithms based on discrete doubly stochastic autoregressions with multiple roots of characteristic equations," In CEUR Workshop Proc., Vol. 2076, pp. 19-29, 2018.

[25] I.D. Melo and M. P. Antunes, "Microgrid state and frequency estimation using Kalman filter: an approach considering an augmented measurement Jacobian matrix," Elec. Eng., Vol. 104, pp. 3523-3534, 2022.

[26] S. Parkinson, H. Ringer, K. Wall, E. Parkinson, L. Erekson, D. Christensen, and T.J. Jarvis, "Analysis of normal-form algorithms for solving systems of polynomial equations," J. Comput. Appl. Math., Vol. 411, pp. 114235(1-19), 2022.

[27] S.H. Strogatz, *Nonlinear dynamics and chaos: with applications to physics, biology, chemistry, and engineering*, CRC press, 2018.

[28] W. Zhang, L. Da, Q. Sun, L. Zhang, and W. Guo, "HOPF bifurcation and stability conditions for a class of nonlinear mass

regulation systems with delay," Ocean Eng., Vol. 238, pp. 109665(1-8), 2021.

[29] K. Atkinson and W. Han. *Theoretical numerical analysis*, Springer, Vol. 39, pp. xvii+-576, 2005.

[30] S. Wieczorek, B. Krauskopf, T. B. Simpson, and D. Lenstra, "The dynamical complexity of optically injected semiconductor lasers," Phys. Rep., Vol. 416, pp. 1-128, 2005.

[31] A. Jafari, KH. Mabhouti, and M.H. Heydarabad, "Effect of the External Mirror Feedback Strength in the Dynamics and Spectrum of the Injected Semiconductor Lasers," Brazil. J. Phys., Vol. 44, pp. 8-18, 2014.

[32] D. Zhong, H. Yang, J. Xi, N. Zeng, and Z. Xu, "Exploring new chaotic synchronization properties in the master-slave configuration based on three laterally coupled semiconductor lasers with self-feedback," Opt. Exp., Vol. 28, pp. 25778-25794, 2020.

[33] M. Cheng, C. Luo, X. Jiang, L. Deng, M. Zhang, C. Ke, S. Fu, M. Tang, P. Shum, and D. Liu, "An electrooptic chaotic system based on a hybrid feedback loop," J. Lightw. Technol., Vol. 36, pp. 4259-4266, 2018.

[34] N. Jiang, W. Pan, B. Luo, L. Yan, S. Xiang, L. Yang, D. Zheng, and N. Li, "Properties of leader-laggard chaos synchronization in mutually coupled external-cavity semiconductor lasers," Phys. Rev. E, Vol. 81, pp. 066217(1-9), 2010.

[35] N. Jiang, W. Pan, L. Yan, B. Luo, X. Zou, S. Xiang, L. Yang, and D. Zheng, "Multiaccess optical chaos communication using mutually coupled semiconductor lasers subjected to identical external injections," IEEE Photon. Technol. Lett., Vol. 22, pp. 676-678, 2010.

[36] J. Ohtsubo, *Dynamics in semiconductor lasers with optical injection. Semiconductor Lasers: Stability, Instability and Chaos*. Berlin, Heidelberg, Springer, pp. 169-204, 2012.

Erfan Abbaszadeh Jabal Kandi is a PhD candidate of Physics in the Department of Physics, Urmia University, Urmia, Iran. He is working on semiconductor laser systems and their applications.

Khosro Mabhouti is an assistant professor of physics in the Department of Physics, Urmia University, Urmia, Iran. Linear and nonlinear optics and laser dynamics are some of his research areas.

Rahim Naderali is an assistant professor of physics in the Department of Physics, Urmia University, Urmia, Iran. Quantum optics and laser dynamics are some of his research areas.

Neda Samadzadeh is a PhD candidate of Physics in the Department of Physics, Urmia University, Urmia, Iran. She is working on semiconductor laser systems and numerical modeling.